MSDE

PAPER

View Article Online
View Journal | View Issue

Cite this: *Mol. Syst. Des. Eng.*, 2022, 7, 1093

Changing the surface properties with a "click": functionalization of DLP-printed structures exploiting residual acrylate functions

Andrea Cosola,[ab] Annalisa Chiappone *[c] and Marco Sangermano [b]

Received 7th April 2022,
Accepted 19th May 2022

DOI: 10.1039/d2me00059h

rsc.li/molecular-engineering

The presence of residual acrylate functions on the surface of DLP-printed objects produced from formulations containing multifunctional monomers is here taken as a potential advantage for post-functionalization purposes. The unreacted acrylates exposed on the surface of printed parts are used as active sites for surface-modification, exploiting the selectivity of the aza-Michael and thiol–ene "click" reactions towards C=C bonds and their ability to yield regiospecific products under mild conditions. By following this versatile approach, the surface wettability is easily tuned by grafting either hydrophobic or hydrophilic functionalities. This allows achieving surfaces with water contact angles ranging from ~22° to ~106°, by simply playing with the surface chemistry but starting from the same DLP-printed substrate. Also, surface thiolation is explored to generate an active interface suitable for the surface-anchoring of photogenerated AgNPs. Such a strategy of post-printing functionalization may further extend the possibilities given by 3D-printing, because it can allow the implementation of special functions to printed parts without the need to introduce any additional component to the printable formulation.

Design, System, Application

3D-printing is radically changing the manufacturing paradigms, becoming a hot topic in the academic and industrial fields. Among the different printing techniques, vat printing represents a versatile option to produce precise, functional objects. The development of new vat-printable and functional materials has been widely investigated but the possibility to fully exploit the polymer chemistry and reactivity to further modify the surface properties of 3D printed objects represents a step forward, extending the horizons of vat polymerization. Here, the incomplete double bond conversion derived from the DLP-printing of multifunctional monomers was exploited for post-printing surface modifications. The aza-Michael and thiol–ene reactions were successfully employed to tune, as a proof of concept, the hydrophilicity/phobicity of the printed parts by taking advantage of the unreacted acrylate functionalities exposed on their surface. Moreover, the surface-anchoring of photo-reduced silver nanoparticles was also induced. The versatility given by this approach opens a path for the easy tuning of several surface properties. In this sense, future studies may be focused on the selective modification of 3D printed microfluidic devices or on the design of components for biomedical applications exploiting the well-known antibacterial properties of silver-patterned surfaces.

1 Introduction

The term 3D-printing refers to a wide range of revolutionary technologies that enable the layer-by-layer fabrication of sophisticated objects starting from digital CAD models.[1,2] Given the possibility to process materials without the need for expensive moulds or machining, with low waste and an almost unlimited freedom of customization, 3D-printing is radically changing the manufacturing paradigms, becoming a hot topic in both the academic and industrial fields.[3,4]

This reflected into the development of several types of 3D-printers that mainly differ in terms of working principle and material feedstock. Just focusing on polymers, some machines extrude preheated thermoplastic filaments, others exploit lasers to sinter thermoplastic powders together and still others allow printing thermosets *via* the photopolymerization of a liquid resin.[5,6] The latter especially, grouped under the blanket term "vat polymerization", have become increasingly popular due to the possibility to tune the structural properties of printed parts by means of spatiotemporally controlled photochemical reactions. This allows the fabrication of even more complex architectures with a finer accuracy.[7]

However, many practical applications have given attention to not only the production of customized and complex structures, but also the engineering of materials to meet special requirements. In this regard, the use of functional

[a] *National Interuniversity Consortium of Materials Science and Technology (INSTM), Via G. Giusti 9, Florence 50121, Italy*
[b] *Department of Applied Sciences and Technology, Politecnico di Torino, C.so Duca degli Abruzzi 24, Turin 10129, Italy*
[c] *Department of Chemical and Geological Sciences, Università degli Studi di Cagliari, Via Università 40, 09124 Cagliari, Italy.*
E-mail: annalisa.chiappone@unica.it

materials, the design of topological architectures and the development of functionalization methods such as surface modifications may be significant strategies to extend the possibilities given by 3D-printing. In particular, the post-printing modification of polymeric surfaces opened-up new horizons in many different fields.[8–10] Indeed, this approach is highly desirable because it offers the opportunity to impart superior functionalities to printed parts, *e.g.* biocompatibility,[11–13] antifouling,[14] tuneable wettability,[15–17] and antibacterial[18] and electrical properties,[19,20] in a cost-effective manner and without affecting the bulk properties.

Looking at vat polymerization, chemical moieties containing the desired reactive groups can be mixed within photocurable resin to be later exploited for post-printing surface functionalization. Roppolo *et al.*[21] prepared off-stoichiometric thiol–yne formulations to print structures displaying unreacted triple bonds on their surface which serve as active sites for selective functionalization. Wang *et al.*[17,20] integrated a printable resin with a vinyl-terminated initiator to obtain functional materials which can be easily post-functionalized *via* surface-initiated atom transfer radical polymerization. Stassi *et al.*[22] functionalized the surface of micro-objects, exploiting the presence of carboxylic groups, which resulted from the use of an acrylate-based formulation containing acrylic acid. Likewise, Chiadò *et al.*[23] designed a photocurable formulation containing a controlled number of carboxylic groups that serve to covalently immobilize specific bioreceptors on a 3D-printed device.[23] Besides this rather conventional approach, also the unsaturated functions which remained after the 3D-printing of acrylate-based resins can provide reactive sites for post-printing surface modifications,[24,25] so as to give new functionalities to the printed objects following a "grafting-to" approach.[26,27]

Within this framework, the aim of this work is to explore different surface-modification strategies to benefit from acrylate functions that remained unreacted after the digital light processing (DLP) 3D-printing of a photocurable formulation containing a multi-acrylated cyclodextrin.[28] First, a formulation based on this multifunctional monomer was successfully 3D printed and the acrylate conversion on the surface of DLP-printed parts was evaluated. Then, the aza-Michael and thiol–ene "click" reactions are proposed as versatile tools for post-printing surface-modifications. In particular, the wettability of the printed structures was tuned by anchoring to the surface either hydrophobic or hydrophilic polymer chains. Furthermore, surface thiolation was explored to generate an interface suitable for the surface-anchoring of photo-reduced silver nanoparticles.

2 Results and discussion

As reported in the literature, the photopolymerization of multifunctional (meth)acrylates enables the fast generation of densely crosslinked polymers, but it also entails an incomplete conversion of unsaturated functionalities.[29] Therefore, a residue of (meth)acrylate groups is expected after the DLP-printing of resins containing multifunctional monomers. Nevertheless, taking advantage of the high selectivity of the Michael and thiol–ene reactions towards C=C bonds,[30–35] these residual unsaturated functions can serve as potential active sites for post-printing functionalization.

To prove the feasibility of this strategy, we prepared a photocurable formulation (Fig. 1a) by dissolving a multifunctional γ-cyclodextrin derivative (Ac-γ-CyD, 20 wt%) decorated with 21 acrylate functions[28,36] into the poly(ethylene glycol) diacrylate (PEGDA) oligomer, with Irgacure 819 added as a photoinitiator (PI, 0.2 phr). This is because we expected that such a formulation would allow DLP-printing highly crosslinked thermosets, whilst leaving a significant residue of unreacted acrylate functions to be later exploited for post-printing modifications.

First, the printing parameters were optimized. Following a previous study on the photoreactivity of Ac-γ-CyD based DLP-printable resins,[28] the light intensity and the exposure time were set to 40 mW cm^{-2} and 0.8 s per layer, respectively, while the layer thickness was kept at 50 μm. This allowed printing highly complex 3D-geometries (Fig. 1b) having a good fidelity to the CAD file (displacement from the digital model of about 0.02 mm, corresponding to an average mismatch of 2.2%). Then, gel content (GC) and ATR-FTIR measurements were performed on the printed samples to evaluate their crosslinked fraction and the double bond conversion (DBC), respectively. These tests confirmed that despite the generation of densely crosslinked thermosets (GC = 96.9 ± 0.3%), a significant amount of C=C bonds did not take part in the reaction during the printing step (DBC = 60.5 ± 1.8%).

The incomplete DBC can be ascribed to the complex photopolymerization mechanisms of multifunctional (meth) acrylates. Indeed, as the reaction proceeds, the degree of crosslinking increases so much that the mobility of the polymeric chains is drastically reduced. Therefore, even if highly crosslinked thermosets are generated, the reactivity of the system drops down due to limited radical diffusion and the reaction stops at low DBC values due to early vitrification.[29,37]

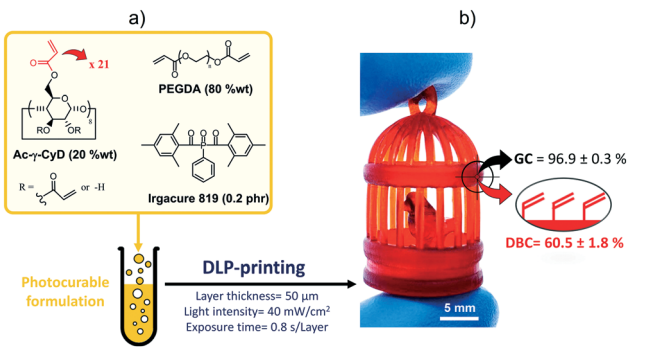

Fig. 1 a) Photocurable Ac-γ-CyD/PEGDA formulation studied in this work, and b) DLP-printed part (methyl red dye added to increase the printing resolution), characterized by a GC close to 97% but with a DBC below 61%.

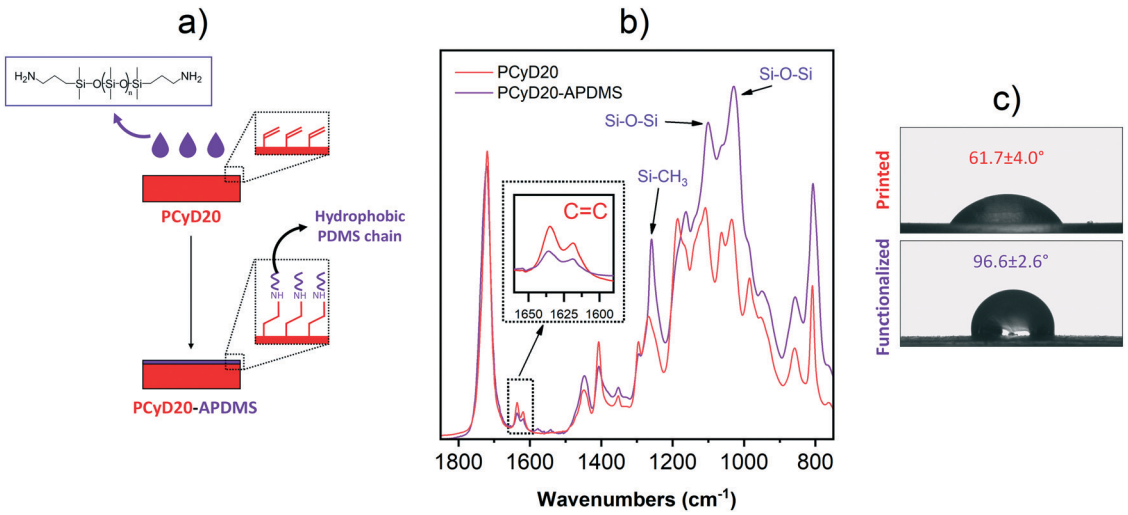

Fig. 2 a) Schematic representation of the surface-grafting of A-PDMS onto the printed sample PCyD20 following the aza-Michael reaction pathway; b) ATR spectra of the printed and functionalized samples, PCyD20 and PCyD20-APDMS, respectively, with a detailed view of the C=C stretching vibration at 1633 cm^{-1} before and after the surface modification and c) water contact angles on the surface of both the printed and functionalized samples.

However, the presence of residual C=C bonds was exploited in this work for post-printing surface modifications. In particular, two different strategies were explored, namely: a) modification of the surface wetting *via* the grafting of either hydrophobic or hydrophilic functionalities and b) patterning of the surface with silver nanoparticles.

2.1 Post-printing modification of the surface wetting

In the first set of experiments, an amino-terminated polydimethylsiloxane (A-PDMS) was grafted to the surface of the printed samples (PCyD20) in order to reduce their water wettability. The samples were immersed in a solution of A-PDMS diluted in isopropanol, where the side terminal amino groups of the polydimethylsiloxane chains undergo selective aza-Michael addition with the C=C bond of the residual acrylate functions exposed on the surface (Fig. 2a).[38] After intense washing, the grafting was first proved by ATR-FTIR spectroscopy. Fig. 2b shows the superimposed ATR spectra of the functionalized sample PCyD20-APDMS and of the printed sample PCyD20. The lower intensity of the peaks corresponding to the C=C stretching vibrations in the

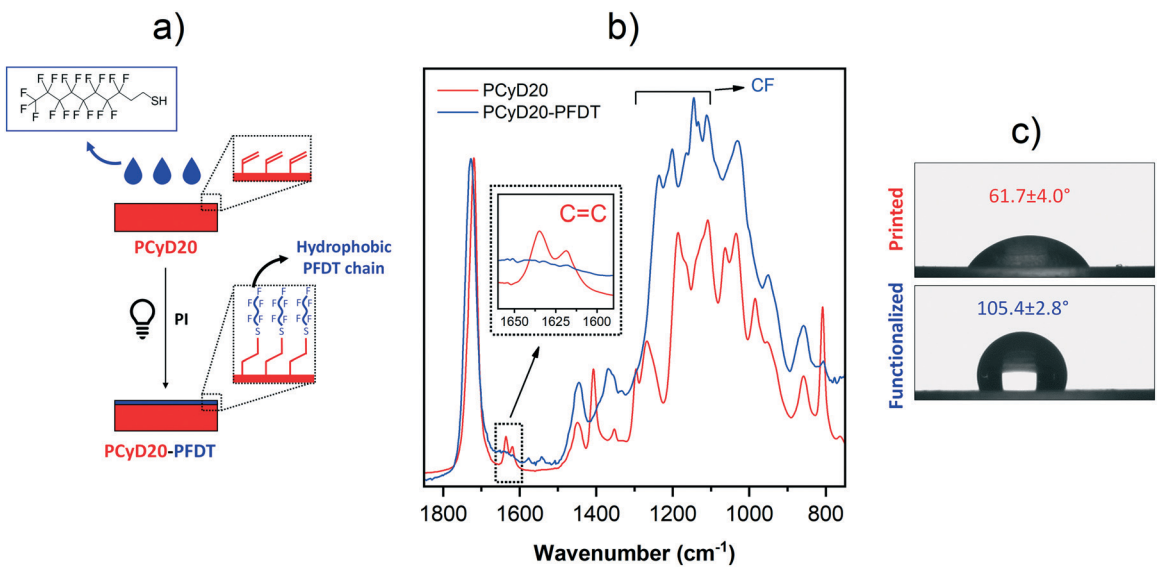

Fig. 3 a) Schematic representation of the surface-grafting of PFDT onto the printed sample PCyD20 following the thiol–ene addition pathway; b) ATR spectra of the printed and functionalized samples, PCyD20 and PCyD20-PFDT, respectively, with a detailed view of the C=C stretching vibration at 1633 cm^{-1} before and after the surface modification and c) water contact angles on the surface of both the printed and functionalized samples.

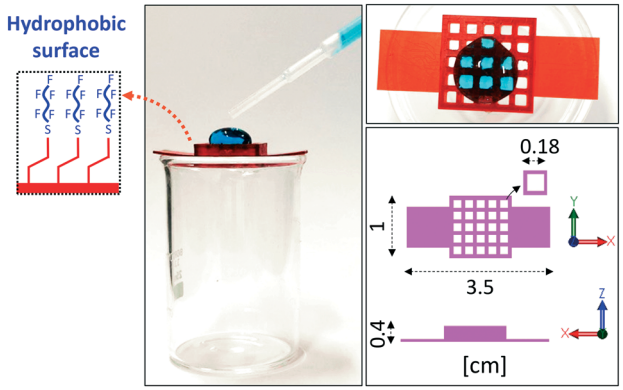

Fig. 4 Photographs of a large water droplet held on a DLP-printed lattice structure after surface functionalization with PFDT.

spectrum of PCyD20-APDMS (see the detailed view of the peak at 1633 cm^{-1} given in Fig. 2b) revealed that the functionalization occurred on the surface of PCyD20.[38] However, a higher conversion of the residual acrylates was not achieved even when using a higher amount of A-PDMS in the grafting solution, probably due to the steric hindrance generated by the high molecular weight PDMS chains. The grafting was further proved by the appearance in the spectrum of PCyD20-APDMS of the characteristic absorption bands of the Si–O–Si and Si–CH_3 vibrations, between 1000 and 1100 cm^{-1} and at 1260 cm^{-1}, respectively.[39] Finally, wettability measurements confirmed that the grafting of A-PDMS increased the hydrophobicity of the printed sample, since the water contact angle (CA) increased from ~62° to ~96° (Fig. 2c).

Moving towards the same goal of generating hydrophobic surfaces, thiol–ene click chemistry[30–33] was then employed to activate the photo-grafting of perfluorodecanethiol (PFDT) to the surface of PCyD20. A few drops of a solution of PFDT in acetonitrile (ACN), containing Irgacure 819 as PI, were spread on the printed sample and the surface grafting was activated by UV-light. Indeed, the light exposure of the thiol-containing perfluorodecane in the presence of a radical PI leads to the generation of a thiyl radical through hydrogen abstraction. Then, the thiyl quickly forms a thioether bond *via* the radical attack of a residual C=C function exposed on the surface of PCyD20 giving a thiol–ene addition product (Fig. 3a), as first confirmed by ATR-FTIR spectroscopy. The ATR spectra of the untreated and treated samples, PCyD20 and PCyD20-PFDT, respectively, are given in Fig. 3b. The spectrum of PCyD20-PFDT revealed an almost total conversion of the residual acrylates located on the surface, since the characteristic peak corresponding to the C=C vibration at around 1633 cm^{-1} nearly disappeared after the surface modification (see detailed view in Fig. 3b).

Moreover, the treated sample shows strong peaks between 1100 and 1300 cm^{-1}, which are ascribable to the –CF_2– and

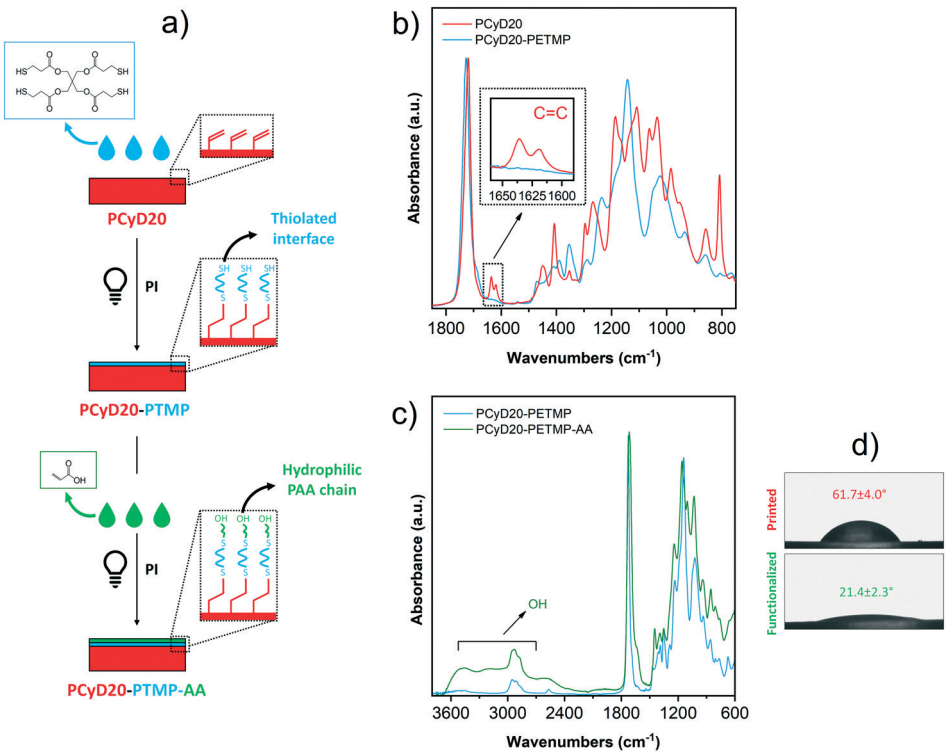

Fig. 5 a) Schematic representation of the thiol–ene addition of PTMP with the residual C=C bonds of the printed sample PCyD20 followed by the thiol–ene addition of AA with free pendent –SH located on the thiolated interface PCyD20-PTMP; b) ATR spectra of the printed and thiolated samples, PCyD20 and PCyD20-PTMP, respectively, with a detailed view of the C=C stretching vibration at 1633 cm^{-1} before and after the surface modification; c) ATR spectra of PCyD20-PTMP before and after the thiol–ene addition with AA and d) water contact angles on the surface of the printed sample before and after the functionalization with AA.

$-CF_3$ vibrations of grafted PFDT chains.[40–42] The successful generation of a fluorinated surface was finally confirmed by the enhanced hydrophobicity of the functionalized samples, as evidenced by the increase of CA from ~62° to ~106° (Fig. 3c).

As a proof of concept, we choose to functionalize with PFDT the surface of a DLP-printed lattice structure. The enhanced hydrophobicity given by the surface modification ensures that water droplets don't permeate through the holes of the structures (Fig. 4).

After having successfully increased the hydrophilicity of the surface of 3D printed parts, the goal of the last set of experiments was, in contrast, to increase the hydrophilic character of the samples. To do this, we developed a surface modification strategy which involves two consecutive thiol–ene reactions (Fig. 5a).

First, a solution of pentaerythritol tetrakis(3-mercaptopropionate) (PETMP) in ACN, with Irgacure 819 added as a radical PI, was applied on the surface of a DLP-printed sample. The surface grafting was initiated by UV-light exposure, leading to the photo-generation of a thiolated interface PCyD20-PETMP that displays free –SH groups, as confirmed by ATR-spectroscopy. Indeed, the peaks corresponding to the C=C stretching vibration were no longer visible in the spectrum of PCyD20-PETMP (see detailed view in Fig. 5b), indicating the total conversion of the residual acrylate functions on PCyD20 after the thiol–ene reaction with PETMP. Furthermore, the presence of free pendent –SH was evidenced by the appearance of a new peak at around 2560 cm^{-1}, typically attributed to the stretching vibration of –SH groups.[43] In this case a tetrafunctional thiol was used aiming to exploit a portion of the four terminal –SH groups for the surface grafting of the molecule by the thiol–ene addition with the residual C=C bonds on the printed part, while leaving the rest of the –SH groups still available for further reaction. Indeed, these free pendent –SH groups were involved in the subsequent thiol–ene addition with acrylic acid (AA) to photo-generate a hydrophilic surface. Thus, a few drops of a solution of AA diluted in ACN and the radical PI Irgacure 819 were dripped onto PCyD20-PETMP, and the surface modification was activated upon exposure to UV-light. The grafting of AA was confirmed by ATR-FTIR spectroscopy, since the typical broad absorption band of the carboxylic acid –OH stretching appeared in the spectrum of the treated sample in the region 3300–2500 cm^{-1} (Fig. 5c).[24,44] Wettability measurements gave additional confirmation of the successful functionalization of the surface with AA, since the samples became much more hydrophilic (CA ~22°, Fig. 5d).

2.2 Post-printing surface patterning with silver nanoparticles

Following a different strategy, the free –SH groups which remained pendent from the thiolated interface generated on PCyD20 (see Fig. 5a) were further exploited as active sites for the anchoring of silver nanoparticles (AgNPs, Fig. 6a). Indeed, thiols can immobilize NPs obtained upon the photo-reduction of transition metals *via* the generation of bridging bonds.[45–47]

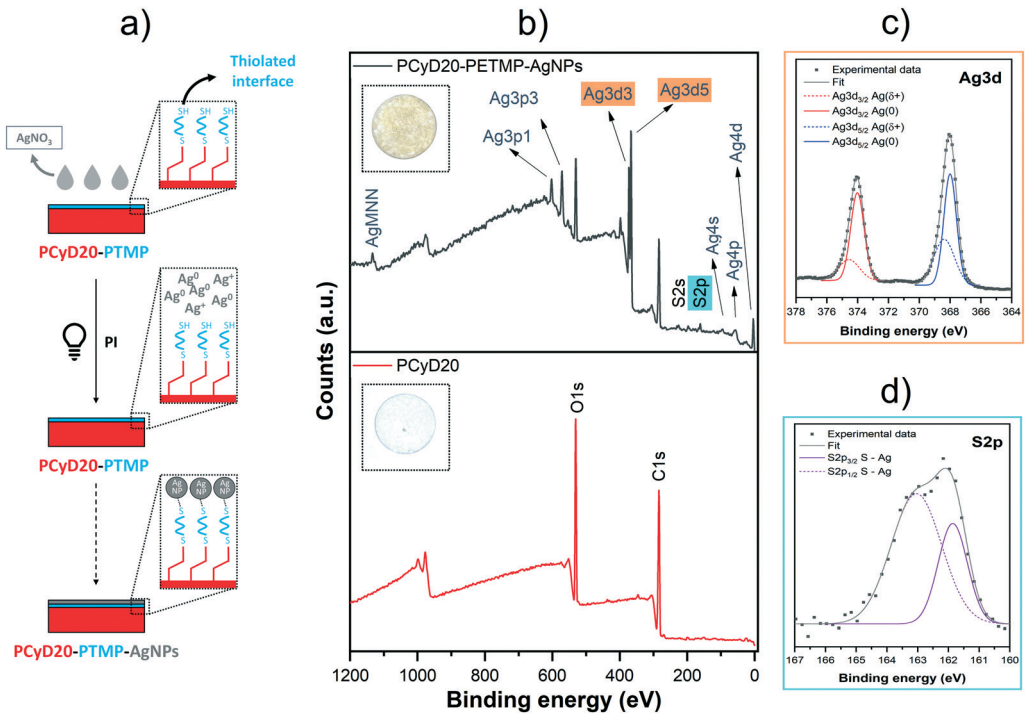

Fig. 6 a) Schematic representation of the photoreduction of Ag ions and the immobilization of AgNPs onto the free pendent –SH groups on the thiolated PCyD20-PETMP interface *via* S–Ag bridging-bonds; b) survey XPS spectra of the printed sample before (PCyD20) and after the photografting of AgNPs (PCyD20-PETMP-AgNPs), with inset photographs of the samples; and high resolution S2p (c) and Ag3d (d) spectra showing the experimental data, the best fitting analysis, and the deconvolution.

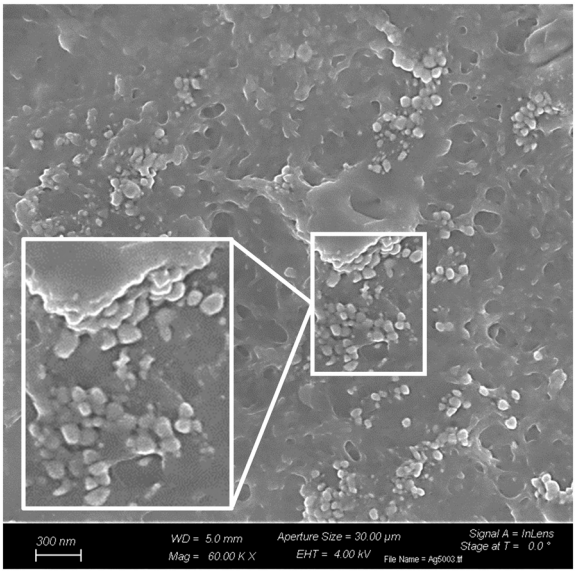

Fig. 7 FESEM micrographs showing clusters of spherical AgNPs on the surface of the thiolated PCyD20-PETMP interface.

Accordingly, the samples previously functionalized with PETMP were immersed in a water solution of $AgNO_3$ (10 wt%), with Irgacure 2959 used as a reducing agent, and the photoreduction of Ag^+ to Ag^0 on the free –SH sites was activated by UV-light. Indeed, it has been demonstrated that the long-lived ketyl radicals generated upon the photolysis of hydroxyketone PIs can promote the reduction of transition metals, including Ag.[48–51] Moreover, the simultaneous oxidation of the benzoyl radicals leads to the production of benzoic acid which contributes to increasing the stability of the NPs.[51]

After washing the samples, the surface of the silver-modified samples became brownish, giving the first qualitative indication of the presence of silver nanoparticles (see insets in Fig. 6b). The anchoring of photo-reduced AgNPs onto the thiolated interface PCyD20-PETMP was investigated with XPS. The survey spectrum of the treated sample PCyD20-PETMP-AgNPs clearly shows the typical peaks corresponding to the binding energy (BE) of Ag atoms in their zerovalent state ($Ag3d_{5/2}$ and $Ag3d_{3/2}$ at 368.1 eV and 374.1 eV, see Fig. 6b).[45–47] Moreover, the fitting analyses of the Ag3d core-level (Fig. 6c) proved that Ag atoms at the surface of the photogenerated NPs are bonded to the surface. Indeed, the peak deconvolution shows two spin–orbit doublets: the contributions with lower BE are conventionally assigned to unperturbed Ag^0 atoms in the NP core, while the ones with higher BE can be attributed to positively charged Ag atoms ($Ag\delta^+$) coupled with the thiolated surface *via* S–Ag bridging-bonds.[45] The deconvolution of the S2p peak further confirmed the generation of S–Ag anchoring sites, since the contribution at 161.85 eV ($S2p_{3/2}$) is conventionally attributed to sulphur atoms chemically bonded to metal atoms at the NP surface (Fig. 6d).[45,46]

The surface patterning with AgNPs was also evidenced by FESEM investigations. Indeed, the micrographs given in Fig. 7 clearly show the presence of clusters of spherical AgNPs on the surface of the functionalized PCyD20-PETMP-AgNP samples.

3 Conclusions

In this study, the incomplete double bond conversion derived from the DLP-printing of a formulation containing multifunctional monomers was exploited for post-printing surface modifications. Indeed, the aza-Michael and thiol–ene reactions were successfully employed to impart special features to the DLP-printed parts by simply taking advantage of the unreacted acrylate functionalities exposed on the surface. First, the wettability of the printed samples was easily tuned by grafting either hydrophobic chains of an amino terminated polydimethylsiloxane and a perfluorodecanethiol, or hydrophilic chains of acrylic acid. The successful functionalizations were confirmed by ATR-spectroscopy and water contact angle measurements. Moreover, the generation of a thiolated interface on the printed samples was successfully exploited for the surface-anchoring of photo-reduced AgNPs, as demonstrated by XPS and FESEM investigations.

Overall, the versatility given by this approach would allow further exploration of chemical routes for the easy surface modification of 3D-printed structures. Therefore, we believe this method of post-printing surface functionalization may further extend the horizons of vat polymerization, since the results reported here proved the possibility of giving special functions to DLP-printed parts without the need to add any specific chemical component to the printable formulation. In this sense, future studies may be focused on the study of the selective modification of the wettability of microfluidic devices or the design of components for biomedical applications exploiting the well-known antibacterial properties of surfaces patterned with AgNPs.

4 Experimental

Materials

Polyethylene glycol diacrylate (PEGDA, Mn = 250 g mol^{-1}), bis(3-aminopropyl) terminated poly(dimethylsiloxane) (A-PDMS, Mn = 2500 g mol^{-1}), 1*H*,1*H*,2*H*,2*H*-perfluorodecanethiol (PFDT), pentaerythritol tetrakis(3-mercaptopropionate) (PETMP), acrylic acid (AA), silver nitrate ($AgNO_3$, > 99.0%), ethanol (EtOH), isopropanol (IPA), acetonitrile (ACN), phenylbis(2,4,6-trimethylbenzoyl)phosphine oxide (Irgacure 819), 2-hydroxy-4′-(2-hydroxyethoxy)-2-methylpropiophenone (Irgacure 2959) and methyl red were purchased from Sigma Aldrich and used as received. The multifunctional γ-cyclodextrin derivative Ac-γ-CyD was prepared according to a synthetic protocol already reported in previous studies.[28,52]

Composition of the photocurable formulation and DLP-printing

The printable formulation was prepared by dissolving Ac-γ-CyD (20 wt%) in PEGDA (serving simultaneously as a reactive

diluent and co-monomer) and adding Irgacure 819 (0.2 phr) as a radical photoinitiator.

3D-printing was performed using a MAX X27 DLP-3D printer from ASIGA (building volume of 119 mm × 67 mm × 75 mm, nominal *XY* pixel resolution of 27 μm and a light-emitting diode source at 385 nm). The layer thickness was set to 50 μm, while the light intensity and the exposure time per layer were set to 40 mW cm^{-2} and 0.8 s, respectively. After the printing process, the samples were rinsed in EtOH to remove the unreacted resin before being used for post-printing functionalization purposes.

Disc-shaped samples were DLP-printed (diameter = 12 mm; thickness = 1 mm) and used for post-printing functionalization purposes.

Gel content measurements

Gel content (GC) measurements were performed to evaluate the covalently crosslinked fraction of the printed thermosets. Flat samples (20 mm × 10 mm × 0.5 mm) were prepared by DLP-printing, held in an ultra-fine metal net, weighed, and immersed for 24 h at room temperature (RT) in chloroform to remove un-crosslinked polymers (the soluble fraction). Then, the samples were taken out from the chloroform bath and dried in an oven (80 °C, 6 h). The GC was calculated gravimetrically using the following equation:

$$\mathrm{GC}\ (\%) = \frac{W_\mathrm{d}}{W_0} \times 100$$

where W_d is the weight of the dried sample after solvent extraction and W_0 is the initial weight of the sample.

The measurements were repeated three times and the results averaged.

Post-printing surface modification – grafting of A-PDMS

The printed samples were immersed in a solution of A-PDMS (10 wt%) in IPA for 24 h at RT. Then, the samples were removed from the reaction bath, rinsed under stirring in IPA for 10′ and dried before further characterization.

Post-printing surface modification – photo-grafting of PFDT

A few drops of a solution of PFDT (50% wt) in ACN, with Irgacure 819 added as PI (2% wt, concerning the amount of PFDT), were first spread on the surface of the printed samples and then irradiated for 1 min using a high-pressure mercury Dymax ECE lamp (100 mW cm^{-2}). Then, the samples were rinsed for 10′ in EtOH, to remove unlinked PFDT from the surface, and dried before further characterization.

Post-printing surface modification – photo-grafting of PETMP

A few drops of a solution of PETMP (50% wt) in ACN, with Irgacure 819 added as PI (2% wt, concerning the amount of PETMP), were first spread on the surface of the printed samples and then irradiated for 1 min using a high-pressure mercury Dymax ECE lamp (100 mW cm^{-2}). Then, the samples were rinsed for 10′ in EtOH, to remove unlinked PETMP from the surface, and dried before further characterization. Note that PETMP was appropriately used to leave unreacted thiols (–SH) on the surface for the subsequent thiol–ene addition with AA.

Post-printing surface modification – photo-grafting of AA

A few drops of a solution of AA (10% wt) in ACN with Irgacure 819 added as PI (2% wt, concerning the amount of AA) were spread on the surface of the samples previously functionalized with PETMP and irradiated for 5 min using a high-pressure mercury Dymax ECE lamp (70 mW cm^{-2}). This allows the activation of the thiol–ene reaction *via* the –SH groups remaining on the surface after the first functionalization with PETMP. Then, the samples were triply rinsed in H_2O, to remove the unlinked polyacrylic acid chains, and dried before further characterization.

Post-printing surface modification – photo-grafting of AgNPs

The printed samples already functionalized with PETMP were immersed in a water solution of $AgNO_3$ (10% wt), with Irgacure 2959 added as PI (0.5% wt). Then, the solution was irradiated for 15 min using a Hamamatsu LC8 UV-lamp equipped with an 8 mm light guide (70 mW cm^{-2}), to activate the reduction of Ag ions and the anchoring of the generated AgNPs on the free –SH groups on the thiolated surface. Finally, the samples were rinsed in H_2O for 90 min under sonication and dried before further characterization.

Surface characterization – ATR-FTIR spectroscopy

The measurements were performed using a Nicolet iS50 FT-IR spectrometer (PerkinElmer, Norwalk, CT, USA) equipped with an attenuated total reflectance (ATR) accessory (Smart iTX), to evaluate both the conversion of the acrylate functions after the printing step and the surface chemistry of the printed sample after the post-functionalizations. ATR spectra were collected with a resolution of 4 cm^{-1} between 600 and 4000 cm^{-1}, averaging 32 scans for each spectrum. Data were processed with the Omnic software from Thermo Fisher Scientific.

The surface-DBC of the printed samples was calculated by monitoring the decrease of the peak area of the C=C bond stretching vibration of acrylates at about 1633 cm^{-1} normalized by the constant signal centred at 1730 cm^{-1}, corresponding to the stretching vibration of C=O groups. The measurements were repeated three times and the results averaged.

Surface characterization – contact angle measurements

Water contact angles of the printed samples before and after the different post-functionalizations were determined at RT using a Kruss DSA100 drop shape analyzer, equipped with a video camera and an image software. First, small water droplets (≈15 μL) were applied onto a levelled surface of the printed sample. Then, the static contact angles were

measured using the tangent method. The results were averaged over six measurements for each sample.

Surface characterization – X-ray photoelectron spectroscopy

XPS measurements were performed using a PHI Versaprobe 5000 (Physical Electronics, Chanhassen, MN, USA), equipped with a monochromatic Al K-alpha source (1486.6 eV). Both survey and high resolution (HR) spectra were collected for each sample. The core-level energy shifts were referred to the C 1s peak (C–C) at 284.5 eV. Origin software was used for data analysis and for further peak-fitting procedures.

Surface characterization – FESEM

The morphological characterization of the AgNPs grafted on the surface of the printed samples was performed by using a FESEM Zeiss Supra 40 (Oberkochen, Germany).

Author contributions

Andrea Cosola: investigation, writing of the original draft and editing. Annalisa Chiappone: writing, review and supervision. Marco Sangermano: review and supervision.

Conflicts of interest

The authors declare that they have no known competing financial interests or personal relationships that could have appeared to influence the work reported in this paper.

Acknowledgements

The authors want to thank Fondazione Compagnia di San Paolo for the financial support.

References

1 I. Gibson, D. Rosen, B. Stucker and M. Khorasani, *Additive Manufacturing Technologies*, Springer International Publishing, Cham, 2021.
2 T. D. Ngo, A. Kashani, G. Imbalzano, K. T. Q. Nguyen and D. Hui, *Composites, Part B*, 2018, **143**, 172–196.
3 B. Berman, *Bus. Horiz.*, 2012, **55**, 155–162.
4 S. H. Huang, P. Liu, A. Mokasdar and L. Hou, *Int. J. Adv. Des. Manuf. Technol.*, 2013, **67**, 1191–1203.
5 S. C. Ligon, R. Liska, J. Stampfl, M. Gurr and R. Mülhaupt, *Chem. Rev.*, 2017, **117**, 10212–10290.
6 S. Saleh Alghamdi, S. John, N. Roy Choudhury and N. K. Dutta, *Polymers*, 2021, **13**, 753.
7 A. Bagheri and J. Jin, *ACS Appl. Polym. Mater.*, 2019, **1**, 593–611.
8 Y. Zhang, *Int. J. Bioprint.*, 2017, **3**, 93–99.
9 P. Jiang, Z. Ji, X. Wang and F. Zhou, *J. Mater. Chem. C*, 2020, **8**, 12380–12411.
10 J. Ryan, C. Dizon, C. Catherine, L. Gache, H. Mae, S. Cascolan, L. T. Cancino and R. C. Advincula, *Technol.*, 2021, **9**, 61.
11 B. N. Teixeira, P. Aprile, R. H. Mendonça, D. J. Kelly and R. M. S. M. Thiré, *J. Biomed. Mater. Res., Part B*, 2019, **107**, 37–49.
12 L. R. Jaidev and K. Chatterjee, *Mater. Des.*, 2019, **161**, 44–54.
13 C. Yang, Z. Huan, X. Wang, C. Wu and J. Chang, *ACS Biomater. Sci. Eng.*, 2018, **4**, 608–616.
14 J. D. Castro, E. Carneiro, S. M. Marques, B. Figueiredo, A. J. Pontes, Á. M. Sampaio, I. Carvalho, M. Henriques, P. J. S. Cruz and S. Carvalho, *Surf. Coat. Technol.*, 2020, **386**, 125464.
15 K. M. Lee, H. Park, J. Kim and D. M. Chun, *Appl. Surf. Sci.*, 2019, **467–468**, 979–991.
16 A. C. Weems, K. R. Delle Chiaie, R. Yee and A. P. Dove, *Biomacromolecules*, 2020, **21**, 163–170.
17 X. Wang, X. Cai, Q. Guo, T. Zhang, B. Kobe and J. Yang, *Chem. Commun.*, 2013, **49**, 10064–10066.
18 J. Li, L. Li, J. Zhou, Z. Zhou, X. L. Wu, L. Wang and Q. Yao, *Appl. Mater. Today*, 2019, **17**, 206–215.
19 S. H. Kim, J. A. Jackson, J. S. Oakdale, J. B. Forien, J. M. Lenhardt, J. H. Yoo, S. J. Shin, X. Lepró, B. D. Moran, C. M. Aracne-Ruddle, T. F. Baumann, O. S. Jones and J. Biener, *Chem. Commun.*, 2018, **54**, 10463–10466.
20 X. Wang, Q. Guo, X. Cai, S. Zhou, B. Kobe and J. Yang, *ACS Appl. Mater. Interfaces*, 2014, **6**, 2583–2587.
21 I. Roppolo, F. Frascella, M. Gastaldi, M. Castellino, B. Ciubini, C. Barolo, L. Scaltrito, C. Nicosia, M. Zanetti and A. Chiappone, *Polym. Chem.*, 2019, **10**, 5950–5958.
22 S. Stassi, E. Fantino, R. Calmo, A. Chiappone, M. Gillono, D. Scaiola, C. F. Pirri, C. Ricciardi, A. Chiadò and I. Roppolo, *ACS Appl. Mater. Interfaces*, 2017, **9**, 19193–19201.
23 A. Chiadò, G. Palmara, A. Chiappone, C. Tanzanu, C. F. Pirri, I. Roppolo and F. Frascella, *Lab Chip*, 2020, **20**, 665–674.
24 G. Gonzalez, A. Chiappone, K. Dietliker, C. F. Pirri and I. Roppolo, *Adv. Mater. Technol.*, 2020, **5**, 2000374.
25 R. A. Farrer, C. N. LaFratta, L. Li, J. Praino, M. J. Naughton, B. E. A. Saleh, M. C. Teich and J. T. Fourkas, *J. Am. Chem. Soc.*, 2006, **128**, 1796–1797.
26 S. Minko, in *Polymer Surfaces and Interfaces*, Springer Berlin Heidelberg, Berlin, Heidelberg, 2008, pp. 215–234.
27 B. Zdyrko and I. Luzinov, *Macromol. Rapid Commun.*, 2011, **32**, 859–869.
28 A. Cosola, R. Conti, H. Grützmacher, M. Sangermano, I. Roppolo, C. F. Pirri and A. Chiappone, *Macromol. Mater. Eng.*, 2020, **305**, 2000350.
29 E. Andrzejewska, *Prog. Polym. Sci.*, 2001, **26**, 605–665.
30 A. B. Lowe, *Polym. Chem.*, 2010, **1**, 17–36.
31 C. E. Hoyle, A. B. Lowe and C. N. Bowman, *Chem. Soc. Rev.*, 2010, **39**, 1355–1387.
32 D. P. Nair, M. Podgórski, S. Chatani, T. Gong, W. Xi, C. R. Fenoli and C. N. Bowman, *Chem. Mater.*, 2013, **26**, 724–744.
33 M. Heggli, N. Tirelli, A. Zisch and J. A. Hubbell, *Bioconjugate Chem.*, 2003, **14**, 967–973.
34 A. Y. Rulev, *Russ. Chem. Rev.*, 2011, **80**, 197–218.
35 P. Jonkheijm, D. Weinrich, M. Köhn, H. Engelkamp, P. C. M. Christianen, J. Kuhlmann, J. C. Maan, D. Nüsse, H. Schroeder, R. Wacker, R. Breinbauer, C. M. Niemeyer and H. Waldmann, *Angew. Chem., Int. Ed.*, 2008, **47**, 4421–4424.

36 C. Noè, A. Cosola, A. Chiappone, M. Hakkarainen, H. Grützmacher and M. Sangermano, *Polymer*, 2021, **235**, 124257.
37 K. S. Anseth, K. J. Anderson and C. N. Bowman, *Macromol. Chem. Phys.*, 1996, **197**, 833–848.
38 J. Zhou, X. Allonas, X. Liu and S. Wu, *Polym. Int.*, 2021, **70**, 845–850.
39 Q. Ran, B. Li, D. Sun, H. Yin, Y. Wan, C. Yang, Y. Liu and Y. Mao, *J. Vinyl Addit. Technol.*, 2017, **23**, 305–311.
40 Y. Cheng, A. Barras, S. Lu, W. Xu, S. Szunerits and R. Boukherroub, *Sep. Purif. Technol.*, 2020, **236**, 116240.
41 G. J. W. Aalbers, C. E. Boott, F. D'Acierno, L. Lewis, J. Ho, C. A. Michal, W. Y. Hamad and M. J. MacLachlan, *Biomacromolecules*, 2019, **20**, 2779–2785.
42 X. Yu, Q. Z. Zhong, H. C. Yang, L. S. Wan and Z. K. Xu, *J. Phys. Chem. C*, 2015, **119**, 3667–3673.
43 S. Kuypers, S. K. Pramanik, L. D'Olieslaeger, G. Reekmans, M. Peters, J. D'Haen, D. Vanderzande, T. Junkers, P. Adriaensens and A. Ethirajan, *Chem. Commun.*, 2015, **51**, 15858–15861.
44 M. H. Schneider, H. Willaime, Y. Tran, F. Rezgui and P. Tabeling, *Anal. Chem.*, 2010, **82**, 8848–8855.
45 F. Porcaro, L. Carlini, A. Ugolini, D. Visaggio, P. Visca, I. Fratoddi, I. Venditti, C. Meneghini, L. Simonelli, C. Marini, W. Olszewski, N. Ramanan, I. Luisetto and C. Battocchio, *Materials*, 2016, **9**, 1028.
46 L. Fontana, M. Bassetti, C. Battocchio, I. Venditti and I. Fratoddi, *Colloids Surf., A*, 2017, **532**, 282–289.
47 K. O. Sulaiman, V. Sudheeshkumar and R. W. J. Scott, *RSC Adv.*, 2019, **9**, 28019–28027.
48 S. Jockusch, M. S. Landis, B. Freiermuth and N. J. Turro, *Macromolecules*, 2001, **34**, 1619–1626.
49 J. C. Scaiano, C. Aliaga, S. Maguire and D. Wang, *J. Phys. Chem. B*, 2006, **110**, 12856–12859.
50 M. L. Marin, K. L. McGilvray and J. C. Scaiano, *J. Am. Chem. Soc.*, 2008, **130**, 16572–16584.
51 J. C. Scaiano, K. G. Stamplecoskie and G. L. Hallett-Tapley, *Chem. Commun.*, 2012, **48**, 4798–4808.
52 A. Cosola, R. Conti, V. K. Rana, M. Sangermano, A. Chiappone, J. Levalois-Grützmacher and H. Grützmacher, *Chem. Commun.*, 2020, **56**, 4828–4831.